Propagation Operator Based Boundary Condition for Finite Element Analysis

IEEE Photonics Journal
An IEEE Photonics Society Publication

Open Access

Propagation Operator Based Boundary Condition for Finite Element Analysis

Volume 12, Number 4, August 2020

Keita Morimoto, *Student Member, IEEE*
Akito Iguchi, *Member, IEEE*
Yasuhide Tsuji, *Senior Member, IEEE*

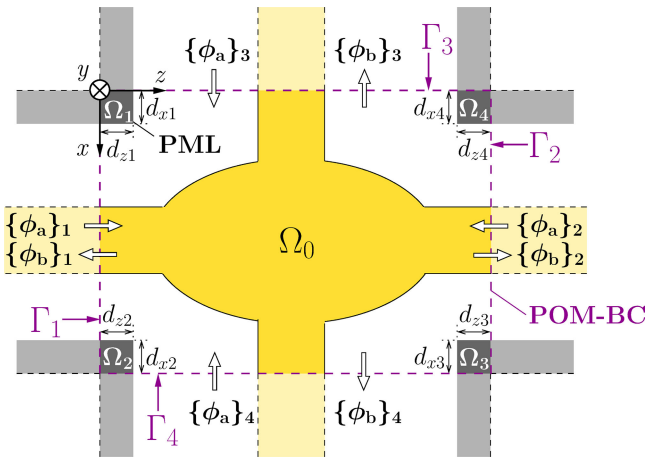

DOI: 10.1109/JPHOT.2020.3015498

Propagation Operator Based Boundary Condition for Finite Element Analysis

Keita Morimoto, *Student Member, IEEE*,
Akito Iguchi, *Member, IEEE*,
and Yasuhide Tsuji, *Senior Member, IEEE*

Division of Information, and Electronic Engineering, Muroran Institute of Technology, Muroran 050-8585, Japan

DOI:10.1109/JPHOT.2020.3015498

Manuscript received June 11, 2020; revised July 18, 2020; accepted August 6, 2020. Date of publication August 11, 2020; date of current version August 25, 2020. This work was supported by JSPS (Japan) KAKENHI under Grant 18K04276. Corresponding author: Yasuhide Tsuji (e-mail: y-tsuji@mmm.muroran-it.ac.jp).

Abstract: A new efficient boundary condition of finite element method (FEM) by using propagation operator is proposed. In this method, input, and output ports are terminated on their own boundaries instead of using perfectly matched layer (PML) which requires expanding the computational window. Moreover, this boundary condition can consider all modes including radiation modes without mode expansion. The propagation operator is efficiently calculated by Denman-Beavers iteration (DBI). The electromagnetic field on the POM boundary can be accurately propagated outside the boundary by using the propagation operator. In addition, we present a technique based on scattering operator method which can reduce the computational complexity of FEM. Three numerical results show that the present scheme is more accurate, and stable than conventional approximate boundary conditions such as using Padé approximation in both TE, and TM modes.

Index Terms: Finite element method (FEM), propagation operator, boundary condition, Denman-Beavers iteration, perfectly matched layer, scattering operator.

1. Introduction

Finite element method (FEM) [1] is one of the most powerful method for analysis and design of optical devices and widely used to understand optical properties of waveguide discontinuities. In order to obtain high accurate results in open system problems with large relative refractive index differences, an appropriate boundary condition which represents arbitrary outgoing electromagnetic fields is required.

A mode expansion technique [2] is used for representing infinite uniform waveguides connected to the input and output ports of finite region. Although this technique can accurately consider both guided and radiation modes, computational cost becomes enormous to calculate the required modes. A simple boundary condition based on the paraxial approximation [3] is usually applied to simple structures. This method requires less computational effort than the mode expansion technique, however, it cannot handle the radiated field components. As an alternative scheme, a boundary condition using Padé approximation [4] has been proposed to be more accurate approach than paraxial approximation, and radiated fields can be evaluated approximately to some extent. In this approach, arbitrariness of propagating field is restricted because the propagation behavior depends on a selected reference refractive index at each boundary. In time-domain analysis,

Mur's absorbing boundary condition (ABC) [5] is also well known and is similar to Padé boundary condition, that is, in frequency domain, second order Mur's ABC corresponds to Padé(1,0) or Fresnel approximation. Although further higher order Mur's ABC has been reported, Mur's ABC also cannot treat wide angle propagation [6]. On the other hand, a perfectly matched layer (PML) [7]–[9] has been introduced for truncating computational windows by absorbing electromagnetic waves while impedance matching conditions are satisfied. Replacing the end of the analysis region by PML, the accurate analysis without mode expansion can be implemented. However, it is necessary to expand the computational window to secure the PML region, and calculation cost becomes high.

Recently, propagation operator method (POM) [10]–[22] has been proposed for waveguide discontinuity problems and it shows good performance for FEM in two- and three-dimensional problems [18]–[22]. This method can deal with all modes at the waveguide discontinuity cross section by calculating square root of the characteristic matrix. In [20], [21], we reported that POM which employs Denman-Beavers iteration (DBI) for calculating the square root matrix can accurately analyze strongly guiding waveguide discontinuity problems which causes a lot of radiation and evanescent waves. It has been reported that Padé approximation which is widely used to obtain the square root matrix so far, suffers from the numerical instability [15]. Although this instability cannot be avoided even though a branch-cut rotation in the complex plane is used in Padé approximation, DBI can stably derive square root matrix via branch-cut rotation. The same situation has occured in full-vectorial FEM [21]. Moreover, instability problem in Padé approximation is more serious when considering very high-index contrast discontinuities such as surface plasmon polaritons (SPPs) waveguides [19]. According to our best knowledge, a boundary condition of FEM using POM has not been reported in the literature previously.

In this paper, we propose efficient and accurate boundary condition of FEM for terminating computational domain by using propagation operator without extra PML absorbing region and any mode expansion. Unlike Padé boundary condition which is based on slowly varying envelope expression and Padé approximation of normal-derivative at the boundary, the proposed boundary condition uses a numerically derived square root matrix. Thus, compared with Padé boundary condition which cannot treat extremely wide angle propagation, the proposed boundary condition can treat all modes including guided, radiation, and evanescent modes. The propagation operator is effectively calculated by DBI. This operator does not need to be recalculated as long as the structure on the port does not vary even if the structure inside the analysis region varies. Moreover, this method can divide entire analysis region to arbitrary smaller regions because electromagnetic fields on the POM boundary can be taken out. If it is connected to a continuous uniform structure, we can obtain propagation characteristics with a slight additional calculation by using the propagation operator. When arbitrary structures are connected in multiple stages, the input-output response of the entire structure can be immediately obtained by constructing the scattering matrices for each structure and calculating its star product [23]. As a result, only the scattering matrix related to structural variation needs to be reconstructed, and that supports efficient design. We derive the input-output response for an arbitrary structure based on the scattering matrix method and examine its validity. In addition, since the previous boundary conditions in [3], [4] has shown only the effectiveness of TE mode, we investigate for both TE and TM modes in this paper. Three numerical results show that the present scheme is more accurate and stable than other approximate boundary conditions such as using Padé approximation in both polarization. This suggestion is an important step to solve problems of computational cost in analysis and design of optical waveguides, and it is promising to extend for three-dimensional boundary conditions.

2. Finite Element Formulation

2.1 Basic Equation

We consider a two-dimensional (2-D) optical waveguide discontinuity problem as shown in Fig. 1, where the computational window is in the xz plane and there is no variation along the y direction

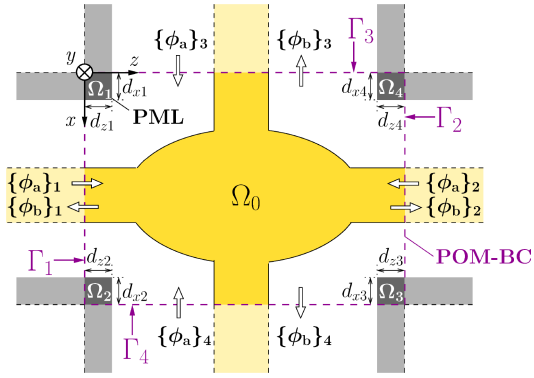

Fig. 1. Schematic diagram of FEM analysis. The analysis region Ω_0 is surrounded by $\Gamma_1 - \Gamma_4$ with POM boundary condition (POM-BC). Outside of the boundaries are assumed to be uniform waveguides.

$(\partial/\partial y = 0)$. The analysis region Ω_0 is surrounded by the boundaries $\Gamma_1 - \Gamma_4$. Since PML which is provided around the outside of the Ω_0 requires expanding the computational window, PML absorber is placed at both ends of the each boundary to be input or output port which are given by the region $\Omega_1 - \Omega_4$ in Fig. 1. From Maxwell's equations, we obtain the following basic equation:

$$s_z \frac{\partial}{\partial x}\left(\frac{p}{s_x}\frac{\partial \Phi}{\partial x}\right) + s_x \frac{\partial}{\partial z}\left(\frac{p}{s_z}\frac{\partial \Phi}{\partial z}\right) + k_0^2 q s_x s_z \Phi = 0 \tag{1}$$

where k_0 is the free space wavenumber, and Φ, p and q are given by

$$\Phi = E_y, \quad p = 1, \quad q = n^2 \quad \text{for TE wave} \tag{2}$$

$$\Phi = H_y, \quad p = 1/n^2, \quad q = 1 \quad \text{for TM wave} \tag{3}$$

where E_y and H_y are y components of electric and magnetic fields, respectively, and n is the refractive index. s_l $(l = x, z)$ represents the PML parameter and the value is taken as

$$s_l = \begin{cases} 1 & \text{in } \Omega_0 \\ 1 - j\,(\rho/d_{li})^2 \tan\delta_i & \text{in } \Omega_i\ (i = 1, 2, 3, 4) \end{cases} \tag{4}$$

where ρ is the distance from the beginning of PML and δ_i is the loss angle at the end of PML $(\rho = d_{li})$.

2.2 FEM Analysis

Dividing the analysis region into quadratic (second-order) triangular elements, the fields Φ within each elements can be approximated as

$$\Phi = \{N\}^T \{\Phi\}_e \tag{5}$$

where $\{N\}$ is the shape function vector for the quadratic triangular element and $\{\Phi\}_e$ is the nodal Φ vector for each element. Applying FEM based on Galerkin method to (1), integrating by parts, considering (5), and assembling the complete matrix for entire analysis region by adding the contributions of all the different elements, we obtain the following matrix equation:

$$[P]\{\Phi\} = \{u\} \tag{6}$$

$$[P] = \sum_e \iint_e \left[p\frac{s_z}{s_x}\frac{\partial\{N\}}{\partial x}\frac{\partial\{N\}^T}{\partial x} + p\frac{s_x}{s_z}\frac{\partial\{N\}}{\partial z}\frac{\partial\{N\}^T}{\partial z} - k_0^2 q s_x s_z \{N\}\{N\}^T \right] dxdz \tag{7}$$

$$\{u\} = \sum_{i=1}^{4} \left(\sum_{e_i}{}' \int_e p \frac{s_l}{s_m} \{\tilde{N}\}_i \frac{\partial \Phi_i}{\partial n_i} dl \right) \tag{8}$$

where the components of vector $\{\Phi\}$ are the values of Φ at all nodal points in entire analysis region, $\sum_e$ extends over all the different elements, and $\sum_{e_i}'$ extends over the elements related to Γ_i. $\{\tilde{N}\}_i$ is the shape function vector for quadratic line element at Γ_i. $\partial/\partial n_i$ represents the partial derivative along the outward normal direction. l and m denote x and z, respectively, when $i = 1$ or 2, switching x and z when $i = 3$ or 4. (6) can also be written in its extended version as

$$\begin{bmatrix} [P]_{00} & [P]_{01} & [P]_{02} & [P]_{03} & [P]_{04} \\ [P]_{10} & [P]_{11} & [P]_{12} & [P]_{13} & [P]_{14} \\ [P]_{20} & [P]_{21} & [P]_{22} & [P]_{23} & [P]_{24} \\ [P]_{30} & [P]_{31} & [P]_{32} & [P]_{33} & [P]_{34} \\ [P]_{40} & [P]_{41} & [P]_{42} & [P]_{43} & [P]_{44} \end{bmatrix} \begin{bmatrix} \{\Phi\}_0 \\ \{\Phi\}_1 \\ \{\Phi\}_2 \\ \{\Phi\}_3 \\ \{\Phi\}_4 \end{bmatrix} = \begin{bmatrix} \{0\} \\ [\tilde{M}]_1\{\Psi\}_1 \\ [\tilde{M}]_2\{\Psi\}_2 \\ [\tilde{M}]_3\{\Psi\}_3 \\ [\tilde{M}]_4\{\Psi\}_4 \end{bmatrix} \tag{9}$$

with

$$[\tilde{M}]_i = \sum_{e_i}{}' \int_e p s_l \{\tilde{N}\}_i \{\tilde{N}\}_i^T dl \tag{10}$$

$$\{\Psi\}_i = \left. \frac{d\{\Phi\}_i}{dn_i} \right|_{\Gamma_i} \tag{11}$$

where $[\tilde{M}]_i$ constructed by the line elements is a finite element mass matrix for eigenmode analysis on the boundary Γ_i.

2.3 POM Boundary Condition

In POM, $\{\Phi\}_i$ $(i = 1, 2, 3, 4)$ is governed by the following equation:

$$\frac{d^2\{\Phi\}_i}{dn_i^2} + [Q]_i^2\{\Phi\}_i = \{0\} \tag{12}$$

where $\{0\}$ is the null vector, and $[Q]_i$ is the characteristic matrix of each boundary written by

$$[Q]_i = \sqrt{[\tilde{M}]_i^{-1}[\tilde{K}]_i} \tag{13}$$

$$[\tilde{K}]_i = \sum_{e_i}{}' \int_e \left[k_0^2 q s_l \{\tilde{N}\}_i \{\tilde{N}\}_i^T - p \frac{1}{s_l} \frac{d\{\tilde{N}\}_i}{dl} \frac{d\{\tilde{N}\}_i^T}{dl} \right] dl \tag{14}$$

where $[\tilde{K}]_i$ constructed by the line elements is a finite element stiffness matrix for eigenmode analysis on the boundary Γ_i. As a solution of the differential equation (12), $\{\Phi\}_i$ can be formally expressed as

$$\{\Phi\}_i = \{\phi_a\}_i \exp(j[Q]_i n_i) + \{\phi_b\}_i \exp(-j[Q]_i n_i) \tag{15}$$

where $\{\phi_a\}_i$ and $\{\phi_b\}_i$ represent vectors standing for backward and forward propagation fields, respectively, under the condition that the outward normal direction of the boundary is positive. Differentiating (15) and eliminating $\{\phi_b\}_i$, we obtain

$$\left. \frac{d\{\Phi\}_i}{dn_i} \right|_{\Gamma_i} = j2[Q]_i \{\phi_a\}_i \exp(j[Q]_i n_i) - j[Q]_i \{\Phi\}_i. \tag{16}$$

Assuming that the incident plane is Γ_1 and is set as the phase reference ($n_1 = 0$), $\{\Psi\}_i$ in (11) can be expressed as

$$\{\Psi\}_i = \begin{cases} j2[Q]_1\{\phi_a\}_1 - j[Q]_1\{\Phi\}_1 & (i=1) \\ -j[Q]_i\{\Phi\}_i & (\text{else}) \end{cases} \tag{17}$$

where $\{\phi_a\}_1$ is the incident field. From (9) and (17), we obtain the following final matrix equation:

$$\begin{bmatrix} [P]_{00} & [P]_{01} & [P]_{02} & [P]_{03} & [P]_{04} \\ [P]_{10} & [\tilde{P}]_{11} & [P]_{12} & [P]_{13} & [P]_{14} \\ [P]_{20} & [P]_{21} & [\tilde{P}]_{22} & [P]_{23} & [P]_{24} \\ [P]_{30} & [P]_{31} & [P]_{32} & [\tilde{P}]_{33} & [P]_{34} \\ [P]_{40} & [P]_{41} & [P]_{42} & [P]_{43} & [\tilde{P}]_{44} \end{bmatrix} \begin{bmatrix} \{\Phi\}_0 \\ \{\Phi\}_1 \\ \{\Phi\}_2 \\ \{\Phi\}_3 \\ \{\Phi\}_4 \end{bmatrix} = \begin{bmatrix} \{0\} \\ 2[C]_1\{\phi_a\}_1 \\ \{0\} \\ \{0\} \\ \{0\} \end{bmatrix} \tag{18}$$

with

$$[C]_i = j[\tilde{M}]_i[Q]_i \tag{19}$$

$$[\tilde{P}]_{ii} = [P]_{ii} + [C]_i \quad \text{for } i = 1 \text{ to } 4. \tag{20}$$

In order to evaluate the propagation property, input mode and output mode are calculated by FEM with quadratic line elements.

For obtaining characteristic matrix $[Q]_i$, DBI [21] which is an iterative scheme based on a recurrence formula is employed and is given as follows:

$$[A]_{i,k+1} = \frac{[A]_{i,k} + [B]_{i,k}^{-1}}{2} \tag{21}$$

$$[B]_{i,k+1} = \frac{[B]_{i,k} + [A]_{i,k}^{-1}}{2} \tag{22}$$

$$[A]_{i,0} = [\tilde{M}]_i^{-1}[\tilde{K}]_i \tag{23}$$

$$[B]_{i,0} = [I] \tag{24}$$

where $[A]_{i,0}$ and $[B]_{i,0}$ represent initial values of the iterations, $[I]$ is the unit matrix and k is a number of iterations. $[A]_{i,k}$ and $[B]_{i,k}$ converge $[Q]_i (= \sqrt{[A]_{i,0}})$ and $[Q]_i^{-1}$, respectively, for sufficiently large k. Here, in order to avoid the instability of the DBI due to the initial matrix with nonpositive real eigenvalues, branch-cut rotation technique is introduced to DBI. The target matrix is transformed as

$$\sqrt{[A]_i} = \exp\left(j\frac{\alpha}{2}\right)\sqrt{[A]_i \exp(-j\alpha)} \tag{25}$$

where α is the rotation angle. Hence the DBI is applied to $[A]_i \exp(-j\alpha)$ instead of $[A]_i$.

3. Scattering Operator Approach

Above mentioned analysis must be recalculated the simultaneous linear equations in every cases the incident conditions are changed. On the other hand, once a scattering operator that expresses relation between input and output ports is constructed, we can immediately calculate the reflected and transmitted waves for any incident waves.

First, considering only two ports of Γ_1 and Γ_2 without the incidence condition, (18) can be rewritten as

$$\begin{bmatrix} [P]_{00} & [P]_{01} & [P]_{02} \\ [P]_{10} & [\tilde{P}]_{11} & [P]_{12} \\ [P]_{20} & [P]_{21} & [\tilde{P}]_{22} \end{bmatrix} \begin{bmatrix} \{\Phi\}_0 \\ \{\Phi\}_1 \\ \{\Phi\}_2 \end{bmatrix} = \begin{bmatrix} \{0\} \\ 2[C]_1\{\phi_a\}_1 \\ 2[C]_2\{\phi_a\}_2 \end{bmatrix}. \tag{26}$$

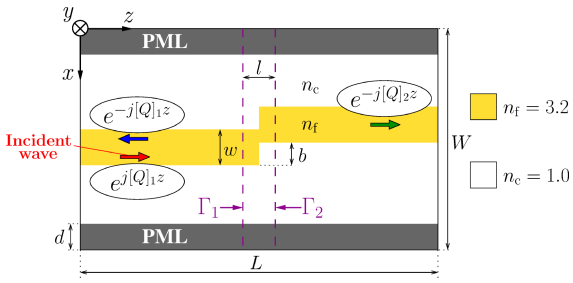

Fig. 2. Schematic of a transverse displacement.

Eliminating $\{\Phi\}_0$ from (26) and considering $\{\Phi\}_i = \{\phi_a\}_i + \{\phi_b\}_i\,(i = 1, 2)$, we obtain,

$$\begin{bmatrix}\{\phi_b\}_1\\ \{\phi_b\}_2\end{bmatrix} = \begin{bmatrix}[S]_{11} & [S]_{12}\\ [S]_{21} & [S]_{22}\end{bmatrix}\begin{bmatrix}\{\phi_a\}_1\\ \{\phi_a\}_2\end{bmatrix} \tag{27}$$

with

$$[S]_{ii} = 2[T]_i^{-1}[C]_i - [I] \tag{28}$$

$$[S]_{ij} = 2[U]_i[T]_j^{-1}[C]_j \tag{29}$$

$$[T]_i = [\tilde{P}_{ii}] - [P_{i0}][P_{00}]^{-1}([P_{0i}] + [P_{0j}][U]_j) \tag{30}$$

$$[U]_i = ([\tilde{P}_{ii}] - [P_{i0}][P_{00}]^{-1}[P_{0i}])^{-1}[P_{i0}][P_{00}]^{-1}[P_{0j}]$$
$$(i, j = 1, 2,\ \ i \neq j). \tag{31}$$

where $[S_{ij}]$ is a component of scattering matrix. If backward wave $\{\phi_a\}_2$ from Γ_2 is negligible, the input-output response can be indicated as

$$\{\phi_b\}_2 = [S]_{21}\{\phi_a\}_1 \tag{32}$$

$$\{\phi_b\}_1 = [S]_{11}\{\phi_a\}_1. \tag{33}$$

4. Numerical Simulation Results

4.1 Transverse Displacement

First, we consider a transverse displacement at the junction of two slab waveguides as shown in Fig. 2, where the refractive indices are $n_f = 3.2$, $n_c = 1.0$, and the structural parameters are set as $W = 4\,\mu$m, $w = 0.2\,\mu$m, $L = 3\,\mu$m, and $d = 0.2\,\mu$m. The domain only in the region within $l = 0.2\,\mu$m including the discontinuity is discretized with triangular meshes. The field at the input and output ends are calculated using the exponential terms in (15). Although eigenvalue decomposition of $[Q]_i (i = 1, 2)$ is additionally required to calculate the exponential terms, there is little influence on the calculation time because it can be computed in parallel with the matrix equation of FEM. Fig. 3 shows electric and magnetic field amplitude in the fundamental TE mode and TM mode, respectively, when, the operating wavelength is $\lambda = 1.55\,\mu$m and a displacement is $b/w = 1$. In Fig. 3(a) and (c), the field distributions are practically the same as the results obtained by placing the PML surrounding the computational domain. In Fig. 3(b) and (d), it can be seen that the field including radiation is accurately propagated from Γ_i to input or output ends by using the exponential terms. Fig. 4(a) and (b) show the relative transmitted and reflected power as a function of b/w, respectively, when the TE fundamental mode is launched. For the sake of comparison, results obtained by paraxial boundary condition (PBC) [3], and Padé boundary condition [4] are also indicated in the same figure. The all results except for the PBC are almost analogous to the results of the PML. On the other hand, in terms of transmitted and reflected powers of the TM

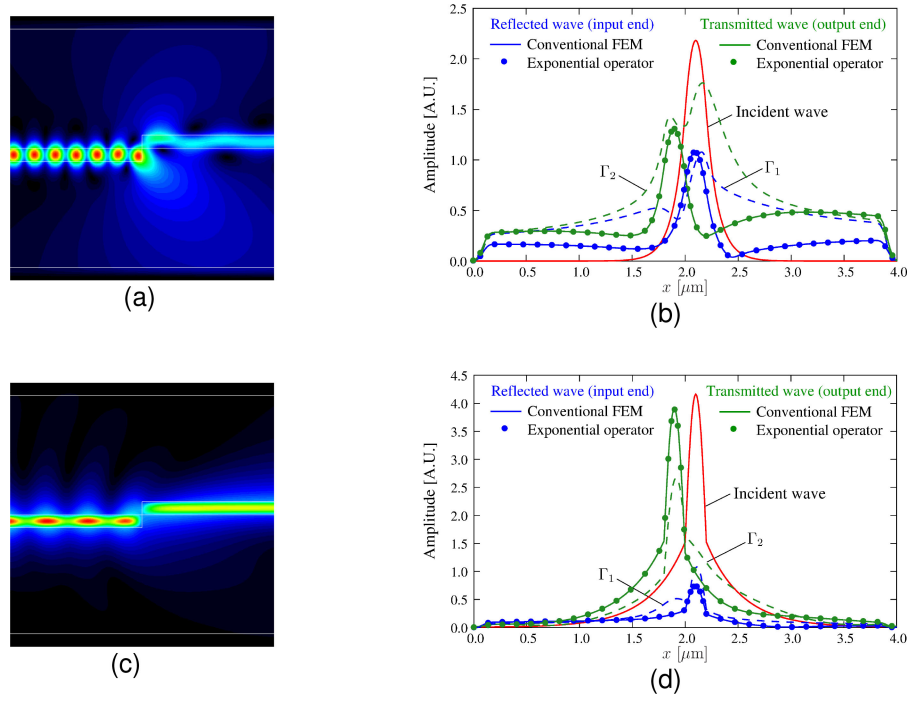

Fig. 3. Propagation field amplitude obtained by FEM analysis with POM boundary conditions corresponding to the problem shown in Fig. 2: Fundamental TE mode: (a) electric field distribution and (b) cross-sectional amplitudes; Fundamental TM mode: (c) magnetic field distribution and (d) cross-sectional amplitudes.

fundamental mode incidence cases shown in Fig. 4(c) and (d), there are significant differences between PML and the conventional boundary conditions. These results also show that increasing Padé order does not always improve accuracy. In addition, it is reported that the higher-order Padé approximation may cause instability even though branch-cut technique is utilized. We think that this is because there are poles corresponding to zeroes in denominator. In our preliminary calculation of these problems, it was confirmed that the higher-order Padé approximation than Padé(3,3) causes unstable behavior in power values and the accuracy could not be guaranteed. Therefore, it can be said that the present method is more accurate and stable than the other approximate boundary conditions for this discontinuity problem.

4.2 Waveguide End Facet

Next, we consider optical radiation problem from an end facet of the waveguide suspended in air as shown in Fig. 5, where the refractive indices are $n_f = 3.6$, $n_c = 1.0$, and the structural parameters are set as $L = 3\,\mu$m, $W = 3.5\,\mu$m, $l = 1.5\,\mu$m, $w = 0.5\,\mu$m, and $d = 0.5\,\mu$m. Fig. 6(a) and (b) show the electric field distributions in the fundamental TE mode incidence and the first-order mode incidence, respectively, for operating wavelength $\lambda = 1.55\,\mu$m. It can be seen that the radiated fields that spread far away are properly terminated by each port. In this case, they propagate as plane-wave-like mode at the output port, and it is relatively easy to analyze even by Padé boundary condition. Considering the case where higher accuracy is required, the structural parameters are changed to $L = 0.2\,\mu$m and $l = 0.1\,\mu$m. For the sake of comparison with conventional FEM which terminates by PML, Fig. 7 shows normalized reflected power as a function of the PML thickness d_z along the propagation direction. From this figure, it can be seen that the PML thickness of $d_z = 0.12\,\mu$m is necessary to secure sufficient convergence. In this case, the calculation time of the

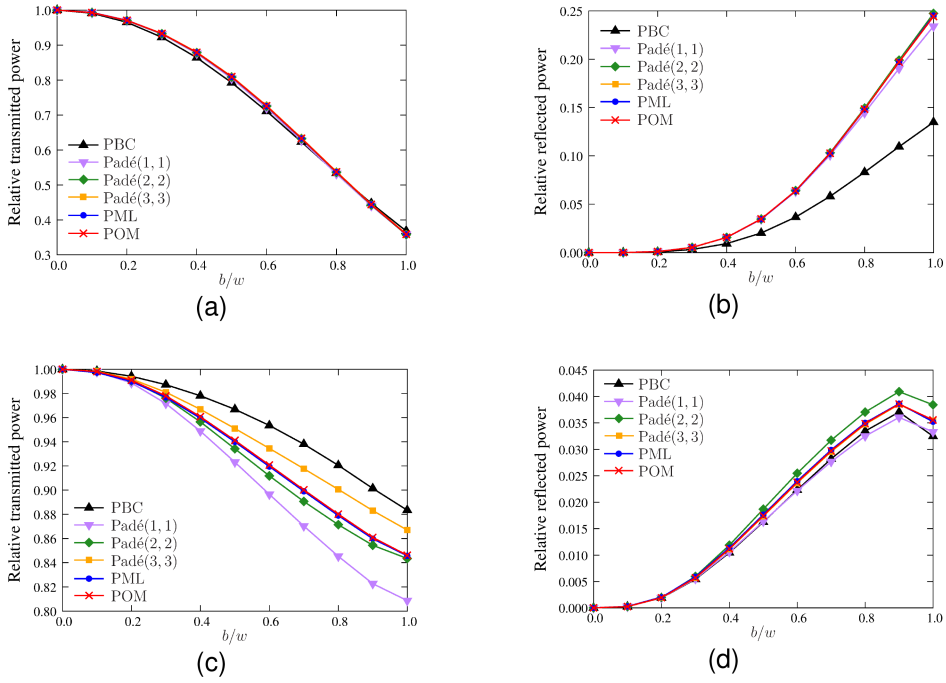

Fig. 4. Relative powers as a function of b/w corresponding to the problem shown in Fig. 2. Fundamental TE mode: (a) transmitted power and (b) reflected power; Fundamental TM mode: (c) transmitted power and (d) reflected power.

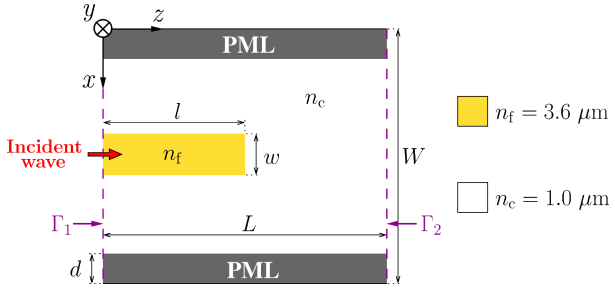

Fig. 5. Optical radiation from end facet of waveguide suspended in air.

Fig. 6. Propagation field distribution obtained by FEM analysis with POM boundary conditions corresponding to the problem shown in Fig. 5: (a) fundamental and (b) first higher order TE modes.

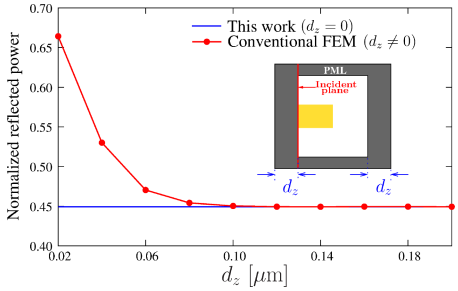

Fig. 7. Normalized reflected power as a function of the PML thickness along the propagation direction.

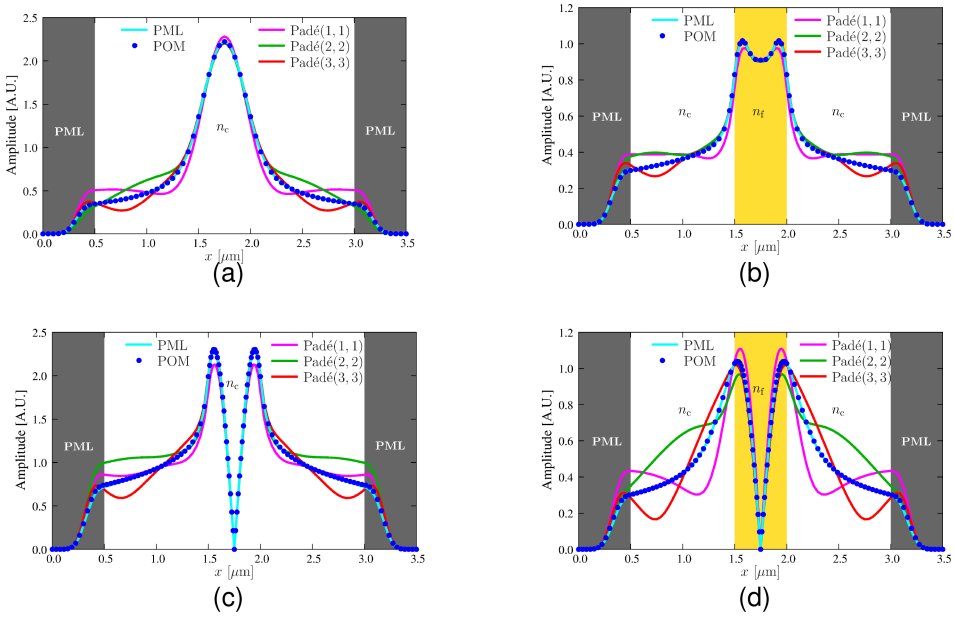

Fig. 8. Cross-sectional electromagnetic field distribution corresponding to the problem shown in Fig. 6. Fundamental TE mode: (a) transmitted wave and (b) reflected wave; Fundamental TM mode: (c) transmitted wave and (d) reflected wave.

linear matrix equation required by the conventional FEM is 2.64 seconds, whereas the presented method is 0.603 seconds. It takes 0.929 seconds to calculate the single propagation operator by 11 iterations of the DBI. Therefore, it can be said that FEM with the new boundary condition can compute faster than conventional FEM. In addition, considering that the structure on each port does not change even if the structure inside the analysis region varies, the propagation operators do not need to be recalculated. It is more effective especially in a optimal design of photonic devices [24]–[26].

Fig. 8 shows the analysis results of the transmitted and reflected amplitude. In order to efficiently calculate the reflected and transmitted waves for the incident waves of the fundamental mode and higher order modes, we employ (32) and (33). It is only necessary to calculate the scattering operator once without solving the linear equation of FEM. While Padé boundary conditions cannot properly evaluate for radiation components even using third-order Padé approximation, the proposed approach is in good agreement with PML boundary conditions.

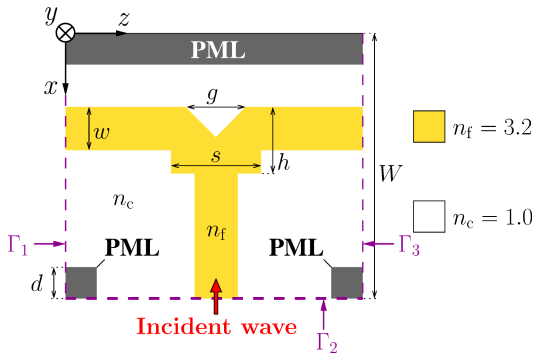

Fig. 9. Schematic of a T-shaped beam splitter.

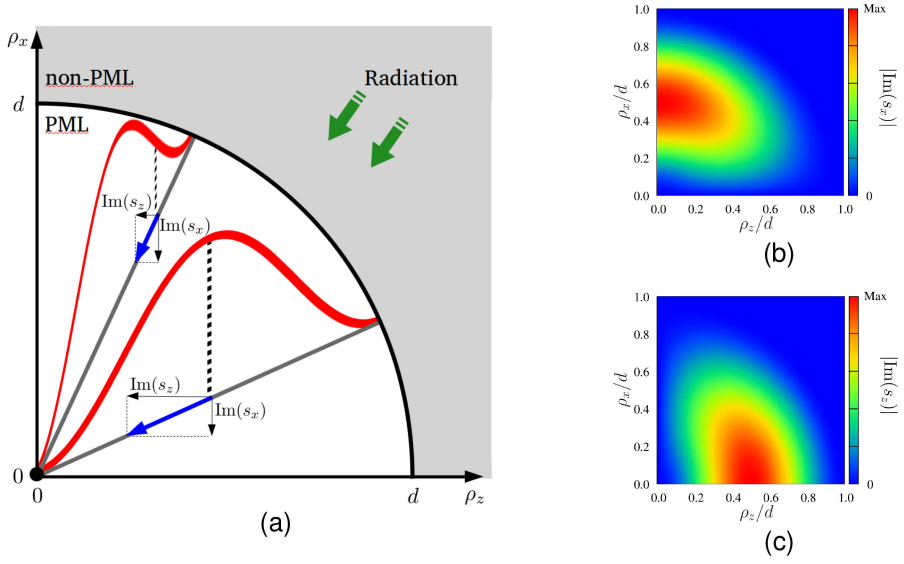

Fig. 10. Modified PML for a corner between two ports. (a) Schematic explanation and the distribution of (b) $|\mathrm{Im}(s_x)|$ and (c) $|\mathrm{Im}(s_z)|$ in relative-coordinate frame.

4.3 T-Shaped Beam Splitter

Finally, we consider a T-shaped beam splitter as shown in Fig. 9 where the refractive indices are $n_f = 3.2$, $n_c = 1.0$, and structural parameters are set as $W = 5\,\mu$m, $w = 0.2\,\mu$m, $h = 0.66\,\mu$m, $s = 1.44\,\mu$m, and $g = 0.87\,\mu$m. Due to the structural symmetry, the transmitted powers are equally distributed in the two outputs. In the analysis of the T-shaped beam splitter in [4], considering that influence of the radiation on the power evaluation is relatively small, stretching parameters of PML at the corners of both ends of input ports were set to 1. However, absorbing conditions for obliquely propagating wave are essential to evaluate including radiation components. If the conventional PML shaped as a rectangle is imposed to a corner of the analysis region, the impedance matching condition is not satisfied. Thus, the distribution of PML stretching parameters are modified as shown in Fig. 10. In order to satisfy the impedance matching condition, the shape of the PML region is made into a circle centered on the corner. The ratio of the imaginary part of the PML coefficient in x- and the z-direction, namely $|\mathrm{Im}(s_i)|$ $(i = x, z)$, corresponds with the magnitude ratio of the x and z components of a vector oriented in the corner. Then, $|\mathrm{Im}(s_i)|$ is increased as the distance from the corner is getting shorter. Since the corner is shared by two ports, s_x and s_z have to be the same value at the corner. Thus we employ cosine function of the distance from the corner to determine

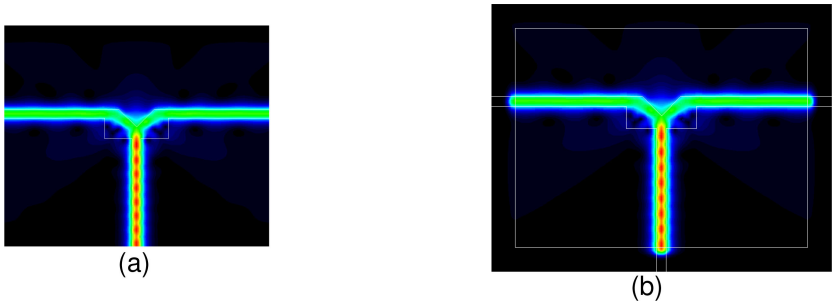

Fig. 11. Propagation field distribution obtained by FEM when the fundamental TE mode is launched. corresponding to the problem shown in Fig. 8. Boundary conditions for input and output ports are (a) POM and (b) PML.

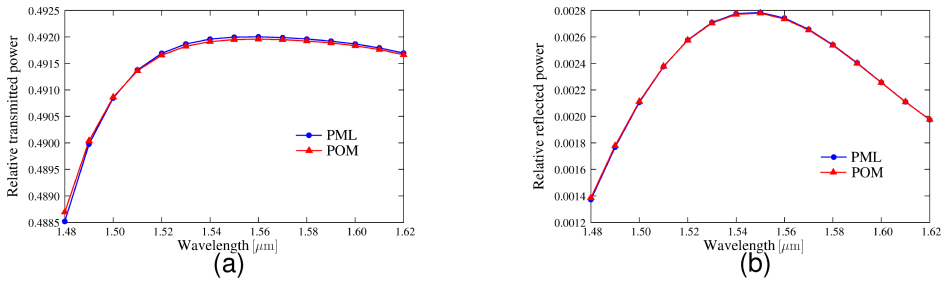

Fig. 12. Comparison of relative (a) transmitted power and (b) reflected power as a function of operating wavelength corresponding to the problem shown in Fig. 8.

the magnitude of absorption, and s_l $(l = x, z)$ is modified as

$$s_l = \begin{cases} 1 & \text{when } R_i > d \\ 1 - j\frac{1}{2}\left[1 - \cos\left(2\pi\frac{R_i}{d}\right)\right]\tan\delta_i\left(\frac{\rho_l}{R_i}\right) & \text{when } 0 \le R_i \le d \end{cases} \tag{34}$$

where R_i is distance from the corner, and ρ_l $(l = x, z)$ is a local coordination shown in Fig. 10(a). Fig. 11(a) and (b) show the electric field distributions obtained by POM boundary conditions and the conventional PML, respectively, when the fundamental TE mode with operating wavelength $\lambda = 1.55\,\mu$m is launched. The field distribution obtained by the PML boundary condition is in good agreement with the PML results including the radiation wave. Fig. 11(a) and (b) show relative transmitted and reflected power as a function of operating wavelength, respectively. While the reflected power is good agreement with PML, the transmitted power is slightly in disagreement. This is because the radiation components generated at the corner between adjacent ports are not sufficiently absorbed, and the reflection from the corners affect the modal power on the ports. This effect can be suppressed by enlarging the corner PML region. In the case of structures which radiation components are relatively large like shown in Fig. 5, radius of the circular PML have to be considerably large. Therefore, the radius and absorption coefficient will need to be selected appropriately depending on the problem. In order to reduce PML region as much as possible aiming the computational efficiency is improved, POM boundary condition can also be imposed on all the planar boundaries, In this case, the modified and approximated PML is required at each end of the PML boundary, that is, around the corner of the computational domain. In the case that strong radiated field reaches the corner of the computational domain, this boundary condition become approximated one. In this paper, in order to derive more reliable scattering matrix operator, we impose PML at the boundary excluding the input and output ends. However, in most of practical cases, we think our POM is applicable to all planar boundaries.

5. Conclusion

In order to improve computational efficiency for analysis of optical waveguides while maintaining its accuracy, we proposed an FEM propagation analysis method using POM as a boundary condition. The propagation operator was computed by DBI. In a numerical example of the transverse displacement, we showed that the proposed method can secure sufficient analysis accuracy in both TE and TM modes, while the PBC and Padé boundary condition are insufficient. In the analysis of the waveguide end facet, using scattering operator approach, reflection and transmission characteristics corresponding to fundamental mode and higher order mode were calculated effectively. It suggests possibility of extension to more efficient analysis by connection of optical waveguides in multiple stages using the scattering operators. In the analysis of T-shaped beam splitter, the evaluation including radiation in proposed method that using modified PML at corners of the analysis region is comparable to conventional PML. We conclude that this method is a powerful boundary condition that reduces computational resources and enables efficient analysis for problems that require high analysis accuracy, and it is promising to extend for three-dimensional boundary conditions. In [21], we have already reported POM for 3-D full-vectorial analysis of waveguide discontinuities using triangular hybrid edge/nodal elements. We think this technique can be readily applicable to express boundary condition in full-vectorial finite element analysis of 3-D waveguide discontinuity problems because the input condition in 3-D full-vectorial FEM with PML has been already expressed using these elements [27], [28]. We think this is probably the most powerful and simple approach and is our future work.

References

[1] M. Koshiba, "Optical waveguide theory by the finite element method," *IEICE Trans. Electorn.*, vol. E97-C, no. 7, pp. 625–635, Jul. 2014.

[2] S. Yoneta, M. Koshiba, and Y. Tsuji, "Combination of beam propagation method and finite element method for optical beam propagation analysis," *J. Lightw. Technol.*, vol. 17, no. 11, pp. 2398–2404, Nov. 1999.

[3] M. I. Davanço, C. E. Rubio-Mercedes, and H. E. Hernandez-Figueroa, "Novel boundary condition for the finite-element solution of arbitrary planar junction," *IEEE Photon. Technol. Lett.*, vol. 13, pp. 46–47, Jan. 2001.

[4] C. E. Rubio-Mercedes, and H. E. Hernandez-Figueroa, "Padé boundary conditions for the finite-element modeling of arbitrary planar junctions," *J. Lightw. Technol.*, vol. 22, no. 2, pp. 669–676, Feb. 2004.

[5] G. Mur, "Absorbing boundary conditions for the finite-difference approximation of the time-domain electromagnetic-field equations," *IEEE Trans. Electromag. Compat.*, vol. EMC-23, no. 4, pp. 377–382, Nov. 1981.

[6] C. Jun, H. Wei, and C. Yiyuan, "Novel Mur condition in frequency domain and its application," *J. Electron. (China)*, vol. 13, pp. 257–266, 1996.

[7] Ü. Pekel and R. Mittra, "An application of the perfectly matched layer (PML) concept to the finite element method frequency domain analysis of scattering problems," *IEEE Microwave Guided Wave Lett.*, vol. 5, no. 8, pp. 258–260, Aug. 1995.

[8] M. Koshiba, Y. Tsuji, and S. Sasaki, "High-performance absorbing boundary conditions for photonic crystal waveguide simulations," *IEEE Microw. Wireless Components Lett.*, vol. 11, no. 4, pp. 152–154, Apr. 2001.

[9] Y. Tsuji and M. Koshiba, "Finite element method using port truncation by perfectly matched layer boundary conditions for optical waveguide discontinuity problems," *J. Lightw. Technol.*, vol. 20, no. 3, pp. 463–468, Mar. 2002.

[10] G. R. Hadley, "Wide-angle beam propagation using Padé approximant operators," *Opt. Lett.*, vol. 17, no. 20, pp. 1426–1428, Oct. 1992.

[11] Y. P. Chiou and H. C. Chang, "Analysis of optical waveguide discontinuities using Padé approximants," *IEEE Photon. Technol. Lett.*, vol. 9, no. 7, pp. 964–966, Jul. 1997.

[12] H. El-Refaei, I. Betty, and D. Yevick, "The application of complex Pade approximants to reflection at optical waveguide facets," *IEEE Photon. Technol. Lett.*, vol. 12, no. 2, pp. 158–160, Feb. 2000.

[13] H. A. Jamid and M. Z. M. Khan, "3-D full-vectorial analysis of strong optical waveguide discontinuities using Pade approximants," *IEEE J. Quantum Electron.*, vol. 43, no. 4, pp. 343–349, Apr. 2007.

[14] J. Xiao, S. Wu, and X. Sun, "A stable and accurate preconditioner for bidirectional beam propagation method," *IEEE J. Quantum Electron.*, vol. 51, no. 4, Apr. 2015, Art. no. 6100107.

[15] S. Wu, J. Xiao, and X. Sun, "Full-vectorial analysis of optical waveguide discontinuities using Denman-Beavers iterative scheme," *J. Lightw. Technol.*, vol. 33, no. 2, pp. 511–518, Jan. 2015.

[16] S. Wu and J. Xiao, "An efficient semivectorial bidirectional beam propagation method for 3-D optical waveguide structures," *J. Lightw. Technol.*, vol. 34, no. 4, pp. 1313–1321, Feb. 2016.

[17] S. Wu and J. Xiao, "An efficient 3-D semivectorial horizontally wide-angle beam-propagation method," *IEEE J. Quantum Electron.*, vol. 52, no. 9, Sep. 2016, Art. no. 6100308.

[18] S. S. A. Obayya, "Novel finite element analysis of optical waveguide discontinuity problems," *J. Lightw. Technol.*, vol. 22, no. 5, pp. 1420–1425, May 2004.

[19] A. M. A. Said, A. M. Heikal, N. F. F. Areed, and S. S. A. Obayya, "Why do field-based methods fail to model plasmonics?" *IEEE Photon. J.*, vol. 8, no. 5, Oct. 2016, Art. no. 4802613.
[20] K. Morimoto and Y. Tsuji, "Analysis of butt coupling of optical waveguides using propagation operator method based on finite element method," *IEICE Trans. Electron. (Japanese Edition)*, vol. J101-C, no. 5, pp. 210–216, May 2018.
[21] K. Morimoto and Y. Tsuji, "Full-vectorial analysis of optical waveguide discontinuities using propagation operator method based on finite element method," *OSA Continuum*, vol. 2, no. 3, pp. 540–553, Mar. 2019.
[22] K. Morimoto and Y. Tsuji, "Analysis of multiple waveguide discontinuities using propagation operator method and beam propagation method," *IEEE J. Quantum Electron.*, vol. 55, no. 4, Aug. 2019, Art. no. 6100108.
[23] J. Tervo *et al.*, "Efficient Bragg waveguide-grating analysis by quasi-rigorous approach based on Redheffer's star product," *Opt. Commun.*, vol. 198, pp. 265–272, Nov. 2001.
[24] Y. Tsuji, K. Hirayama, T. Nomura, K. Sato, and S. Nishiwaki, "Design of optical circuit devices based on topology optimization," *IEEE Photon. Technol. Lett.*, vol. 18, no. 7, pp. 850–852, Apr. 2006.
[25] Z. Zhang, Y. Tsuji, T. Yasui, and M. Eguchi, "Design of ultra-compact triplexer with function-expansion based topology optimization," *Opt. Express*, vol. 23, no. 4, pp. 3936–3950, Feb. 2015.
[26] A. Koda, K. Morimoto, and Y. Tsuji, "A study on topology optimization of plasmonic waveguide devices using function expansion method and evolutionary approach," *J. Lightw. Technol.*, vol. 37, no. 3, pp. 981–988, Feb. 2019.
[27] Y. Ishizaka, Y. Kawaguchi, K. Saitoh, and M. Koshiba, "Three-dimensional finite-element solutions for crossing slot-waveguides with finite core-height," *J. Lightw. Technol.*, vol. 30, no. 21, pp. 3394–3400, Nov. 2012.
[28] T. Yasui, Y. Tsuji, J. Sugisaka, and K. Hirayama, "Design of three-dimensional optical circuit devices by using topology optimization method with function-expansion-based refractive index distribution," *J. Lightw. Technol.*, vol. 31, no. 23, pp. 3765–3770, Dec. 2013.